Supplementary Information

Lubricating properties of single metal ions at interfaces

Clodomiro Cafolla and Kislon Voïtchovsky

Physics Department, Durham University, Durham DH1 3LE, UK
email: kislon.voitchovsky@durham.ac.uk

Index of content:

1. General cleaning procedures and extended Methods

The AFM measurements are highly sensitive to any contamination which manifests itself in the form of anomalous results and inconsistent data. In order to avoid any contamination of either the sample or the cantilever/tip, all aqueous solutions were prepared using borosilicate glass beakers, cylinders and bottles. The glass material was purchased from Pyrex, Corning, NY, USA. A careful cleaning procedure for each glass container was performed in order to remove any polar and nonpolar contaminant. Four washing steps were carried out sequentially: (i) tap water and soap, followed by rinse with tap water 20 times, (ii) ultra-pure water (18.2 MΩ, Merck Millipore, Billerica, MA, USA), (iii) >98% pure propan-2-ol (Merck Millipore, Billerica, MA, USA), and (iv) ultra-pure water again. The propan-2-ol was used as purchased, without further purification.

The cantilevers were immersed in a bath of ultrapure water, followed by propan-2-ol, and finally ultrapure water, for 60 minutes at each step.

Sample preparation

High-quality V1 muscovite mica was purchased from SPI Supplies (West Chester, PA, USA). Mica discs (12 mm diameter) were attached to a steel plate using epoxy glue (Araldite, Basel, Switzerland). Overnight curing at 65 °C was carefully performed in order to obtain a good thermal contact between the mica disc and the steel plate in temperature controlled experiments. The mica was freshly cleaved with adhesive tape before each experiment and rinsed copiously with ultra-pure water (Water AnalaR NORMAPUR, VWR International Ltd, Leicestershire, UK).

All the solutions were prepared in ultrapure water with 99.9% pure salts purchased from Sigma-Aldrich and used without any further purification (St. Louis, MO, USA).

Solutions with controlled pH were prepared by adding a diluted solution of fuming 37% hydrochloric acid (HCl, Merck Millipore, Billerica, MA, USA) to the desired ionic solution while stirring with a magnetic stirrer and tracking the solution's acidity with a pH meter (Mettler Toledo Columbus, OH, USA). No buffering agent was used to avoid interfering with the measurements. [1,2] In the absence of buffering agent, the pH is susceptible to change rapidly in response to changes in the solution's environment and the care was taken to conduct the experiments immediately after the pH adjustment and at controlled temperature. Testing of the pH was also conducted immediately after conducting experiments so as to ensure stability.

Removal of the K^+ ions initially present at the surface of the muscovite mica

When a fresh surface of mica is revealed, immediately after cleaving, half of the ditrigonal cavities exposed are filled with K^+ ions. The ions originate from the bulk of the crystal where they form a cleavable layer that ensures electrostatic neutrality of the crystal. These K^+ ions can, in principle, interfere with the measurements conducted in this study and we ensured their removal and replacement by the desired ions. We estimate, hereafter, their final concentration in the solution during the different experiments.

The cleaved mica surface is a disc of 12 mm diameter, with a total area of $\sim 4.5\times10^{-4}$ m^2. Considering the area of a hexagonal lattice site ($\sim 2.2\times10^{-19}$ m^2, see Fig. 1f), a total of $\sim 1\times10^{15}$ K^+ ions are initially on the surface. This represents 2 nanomoles of K^+. The surface is then rinsed sequentially 20 times with 100 μl of ultrapure water, and then 40 times with 100 μl of the experimental solution. Dividing the amount of K^+ by the total volume of the rinsing liquid yields a K^+ concentration of ~0.3 μM. This concentration is an overestimate because sequential rinsing is more efficient at removing dissolved species than the single rinsing implicitly assumed in our estimate. Nonetheless, 0.3 μM is four orders of magnitude smaller than the 5 mM metal salt used in our ionic solutions and the probabilty to find a K^+ ion adsorbed at the surface of mica is negligible. In ultrapure water, the lowest concentration of H^+ occurs at the highest pH investigated (5.38) where its concentration is still about 4 times that of K^+. Given the fact that the binding constant of H^+ to mica is an order of magnitude larger than that of monovalent metal ions,[3] we expect a vanishingly small probability to find K^+ ions at the surface of mica even in pure water.

Atomic force microscopy measurements

The measurements were performed using a commercial Cypher ES AFM system (Oxford Instruments, Santa Barbara, CA, USA), equipped with temperature control. Two types of measurements were conducted: shearing and imaging, both described, in detail, in the following two sections. All the experiments were conducted with silicon nitride cantilevers originating from a same wafer (Olympus RC800 PSA, Olympus, Tokyo, Japan) with a nominal flexural spring constant, $k_f = 0.39$ Nm^{-1}. Each cantilever was calibrated using its thermal spectrum[4] and found to have typical stiffness of 0.33 (± 0.05) N m^{-1} and Q-factor of 2.8 ± 0.2 in solution.

Calibration of the torsional cantilever inverse optical lever sensitivity (InvOLS) and spring constant, k_t, is a more demanding procedure[5] and was hence performed only on 5 cantilevers to determine the order of magnitude of k_t and its variability. We found $k_t = 184$ (± 1) N m^{-1}. The

calibration procedure, derived from established methods[5], is described, in detail, in the Supplementary Information, Section 3.

When performing the measurements, the cantilevers and the mica substrate were fully immersed in the aqueous solution for the entire experiment. The temperature of the solution was kept at 25.0 ± 0.1 °C, always at thermal equilibrium. This was achieved by tracking the heating/cooling rate of the temperature control system, assuming equilibrium when rates became constant for >10 minutes. For each set of experiments (series of comparative measurements in different solutions, including imaging and shear force spectroscopy), a same cantilever was used to allow direct comparability. Each series of experiment was repeated several times to obtain, at least, three full sets of measurement in any given solution, with the sets subsequently averaged. For a given series, measurements were first conducted in ultrapure water, followed by monovalent, and then divalent salts due to their ability to bind more strongly to the tip and to the mica.[6] The monovalent ion solutions were tested in no particular order between the different sets in order to minimize the risk of systematic errors. When exchanging solutions within a given series, the tip was thoroughly washed with pure water (20 times with 100 μl) and then with the new solution of interest (40 times with 100 μl). The sample holder was also thoroughly washed using the same procedure and the mica sample freshly cleaved. This ensured that all ions from the previous solutions were removed or replaced by those of the new solution.

In general, particular attention was paid to avoid any possible sources of contamination. Cleaning procedures play a crucial role in this endeavour, and atomic level imaging of the area investigated confirmed the absence of contaminants.[7]

Imaging was conducted primarily to complement and support the main experimental technique of shear-force spectroscopy. Topographical images of the samples were used to acquire sub-nanometre information of the confined Stern layer and the overall hydration landscape of the interface, and to confirm the absence of any undesired contaminant. The AFM was operated in amplitude-modulation using photothermal excitation at a frequency close to the cantilever's resonance. The vertical oscillation amplitude, A, of the tip and the phase, φ, between the driving and the tip oscillation were recorded. During imaging, a feedback loop constantly re-adjusts the distance between the base of the cantilever and the sample so as to keep A constant, while φ can vary freely. The ratio A/A_0, between the free amplitude (away from the surface) and the imaging amplitude was kept as high as possible,[8] with A between 0.8-1.5 nm. When operating

in this regime, atomic level resolution of the interface could be routinely achieved.[7,9,10] Details of the Stern layer and any mesoscale structure could be also resolved (Fig. 1).

Shear-force spectroscopy was used to locally quantify the viscoelastic properties of the nano-confined solutions.[11] In shear-force mode, the AFM effectively functions as a nanoscopic linear rheometer, with sub-nanometre lateral oscillation amplitudes chosen to equate the distance between two adjacent lattice sites for adsorbed ions.[12] Practically, the sample is oscillated laterally at a frequency of 1.1 kHz (below the resonance of the scanner) and with an amplitude of ~0.5 nm. Standard force-distance curves are then acquired, but recording three different signals simultaneously as functions of the extension of the cantilever's base:[11] (i) the cantilever tip vertical deflection which quantifies the confining force applied; (ii) the lateral torsional amplitude, A_t, of the cantilever; and (iii) the associated phase, φ_t (see Supplementary Information Fig. S1). The last two signals were extracted using a lock-in amplifier[11,13] with the imposed sample oscillation as a reference. When the tip is away from the surface, no confinement occurs, $A_t = 0$ and φ_t is undefined. When the tip reaches the surface, A_t increases with the confinement force and φ_t quantifies the viscoelastic response of the confined liquid.
For the small torsional amplitudes used in the present study, the magnitude of the shear-force, F_{shear}, can be modeled as:

$$F_{shear} = A_t k_t \qquad (s1)$$

where k_t is the torsional spring constant of the cantilever.
If $\varphi_t = 0°$, the cantilever torsion is in phase with the lateral oscillation of the sample and the coupling is perfectly elastic. In contrast, if $\varphi_t = \pm 90°$, the coupling is perfectly viscous.[11] It should be noted that in the present case, we neglect any additional phase lag induced by possible delays in the mechanical motion of the oscillating scanner, the latter being assumed to operate in phase with the driving signal. Control measurements using a tip pinned in the sample confirm the validity of this hypothesis, at least within the experimental error.
Measurements were conducted with varying confining pressure, obtained by vertically approaching the base of the tip toward the sample at a speed of 10 nm/s. Shear force spectroscopy curves were acquired over typically five different locations in each solution (at least three) resulting in ~100 shear-force curves that were subsequently averaged. Three independent experiments were performed so as to ensure a convergence testing for the heterogeneity of the ion patterns. Since results can, in principle, be affected by progressive

blunting of the tip, the tip was blunted in a controlled manner at the beginning of the experiments (resulting radius of 15-20 nm), so as to allow more reproducibility. Tip blunting was performed also so as to remove any potential asperities and defects which may result in singularities when performing the shear-force experiments. Selected cantilevers were imaged prior or after the shear-force measurements using electron scanning microscopy for comparison (see Supplementary Information Fig. S4). The ex-situ characterization of the cantilevers showed that the ion species did not play any major role in affecting the tip blunting. Also, no significant change in the probe geometry had taken place after the shearing measurements. An in-situ characterization of the tip geometry would be ideal. Unfortunately, the AFM advantages due to the possibility of locally acquiring direct information on interfacial phenomena are counterbalanced by some difficulties in a perfect control on the probe conditions over the experiments. The quality of the high-resolution images (Fig. 1), collected with blunted tips, confirms, however, that the blunting procedure allows obtaining tips, without any major asperities and defects, but still very sharp.

The data analysis was performed using homemade routines programmed in Igor Pro (Wavemetrics, Lake Oswego, OR, USA) and Python. High-resolution imaging was performed immediately before and after each change of location for shear spectroscopy measurements. This ensured that the results were not affected by any kind of singularities in the substrate.

2. Error analysis

The uncertainty on the temperature was taken to be 0.1°. This is likely an overestimate of the error since the AFM temperature control is an order of magnitude more precise, but it allows for errors due to temperature gradients in the liquid. The error on the pH was 0.07, as specified by the pH meter manufacturer.

The uncertainty on the shear amplitude, shear phase and deflection was taken to be the standard error in each case.

The effective friction coefficients were computed using an orthogonal regression distance Python built-in algorithm.[14] The uncertainty on the effective viscosity were calculated using standard formulae for error propagation.[15] The error on the deflection signal and consequently on the tip sample distance and on the normal force was derived from the z-piezo noise, that accordingly to the manufacturer specifications, is lower than 50 pm. We assumed a noise of 50 pm so as to avoid any underestimation in the value uncertainty.

3. Torsional calibration of the cantilever

The cantilevers used in this study, RC-800-PSA, have a rectangular shape, suitable for calibration with the thermal method.[5,16,17] Calibration was performed with the cantilever and the sample immersed in ultrapure water at 25.0 °C. The torsional thermal spectrum of the cantilever is fitted with a Lorentzian, returning a resonance frequency of 420 ± 5 kHz and a Q-factor of 3.3 ± 0.1 for the first torsional eigenmode. To minimize fitting-related errors, a statistical average was taken over multiple fits, each using a slightly different frequency window around the torsional resonance. The torsional spring constant, k_t, is calculated using:[5]

$$k_t = 0.1592\ \rho\ w^4 L Q\ \omega_0^2 \gamma_i \qquad (s2)$$

where ρ is the water density taken as 997 kg m^{-3},[18] w is the width of the cantilever (nominal value of 20 ± 1 μm used), L its length (nominal value of 100 ± 10 μm used), Q and ω_0 are the Q-factor and the angular resonant frequency, and γ_i is the imaginary part of the hydrodynamic function, calculated from Eq. (21) of ref. [17]. When computing γ_i, the water viscosity was taken as 89 × 10^{-5} Pa s.[19] We found $k_t = 184$ (± 1) N m^{-1}. The value is in good agreement with the value of 157.87 N m^{-1} reported by other researchers on the same type of cantilever.[5] The torsional inverse optical lever sensitivity of detector (InvOLS, nm V^{-1}) is calculated using a method described in ref. [5]:

$$\mathrm{InvOLS} = h\sqrt{\frac{2k_B T}{\pi k_t f_0 P_{DC} Q}} \qquad (s3)$$

where h is the tip height (nominal value of 3.0 ± 0.5 μm used), k_B is the Boltzmann constant, T is the temperature, f_0 is the resonance frequency and P_{DC} is the power spectral density detected for the cantilever at DC. We found an InvOLS value of 2.9 (± 0.6) nm V^{-1}, in good agreement with previous reports that found 1.79 ± 0.16 nm V^{-1} for this type of cantilevers.[5] For comparison, the vertical deflection InvOLS was found to be 22.8 (± 0.5) nm V^{-1}.

The thermal method is a non-contact approach and hence allows easier measurement of the cantilever's characteristics and avoids tip damage or contamination.[5] However, the method has also some disadvantages: (i) dependence on the Q-factor, and the P_{DC} both of which may carry a significant measurement uncertainty; (ii) some dependence on the calibration conditions such as humidity and temperature; and (iii) the need to know the exact shape of the cantilever, an issue if imperfections arise in the manufacturing process.[20] Here, steps were taken to reduce

these sources of error. Multiple fits were performed for accurate determination of Q and P_{DC}. Temperature and humidity were precisely controlled throughout all the experiments. The shape, dimensions and conditions of selected cantilever were independently assessed by electron microscopy analysis (see Section S7).

4. Tip preparation procedure for the shear force measurements

In order to perform reproducible shear-force measurements, it is important for the cantilever's tip to maintain, as much as possible, its shape and size throughout the experiment. Experiments with ultra-sharp tips are likely to see a progressive blunting of the tip apex, leading to a change in the nano-confining area. To overcome this issue, we voluntarily partially blunted our tips prior to shear measurements following a well-controlled procedure. This was done by scanning two consecutive images (256 lines/frame, 1 μm x μm) in contact mode with an applied force of approximately 10 nN and at a scan rate of 2 Hz. This method, also used in other studies,[21] allows for reproducible shear-force measurements while minimizing the necessary tip blunting (radius of curvature < 20 nm after blunting, see section 5 below). The stability of the tip apex shape was confirmed by electron microscopy analysis of randomly selected tips before and after the experiments. The radius of the blunted tip was within manufacturer's specifications. The blunting procedure preserved the tip sharpness and removed all the undesired asperities and singularities.

5. Representative results of the raw output signals

Figure S1 presents an example of the raw data obtained from a shear-force measurement experiment, here in a RbCl solution (5.0 mM, pH 5.38, 25.0 °C). The vertical deflection of the cantilever, the shear amplitude and the phase are acquired simultaneously as functions of the Z-piezo extension, the position of the cantilever's base that is moving towards the sample's surface. The zero extension is defined as the point where the tip begins to experience a continuous vertical deflection, loosely interpreted as the point of contact between the tip and the sample. This is an arbitrary definition since no absolute measurement of the surface's height is possible with AFM. In this interpretation, positive values of the base extension represent the true tip-sample distance, whereas negative values indicate the region where the tip does not

move vertically (except for eventual deformation), but the applied force F increases proportionally to the deflection, obeying Hooke's law.

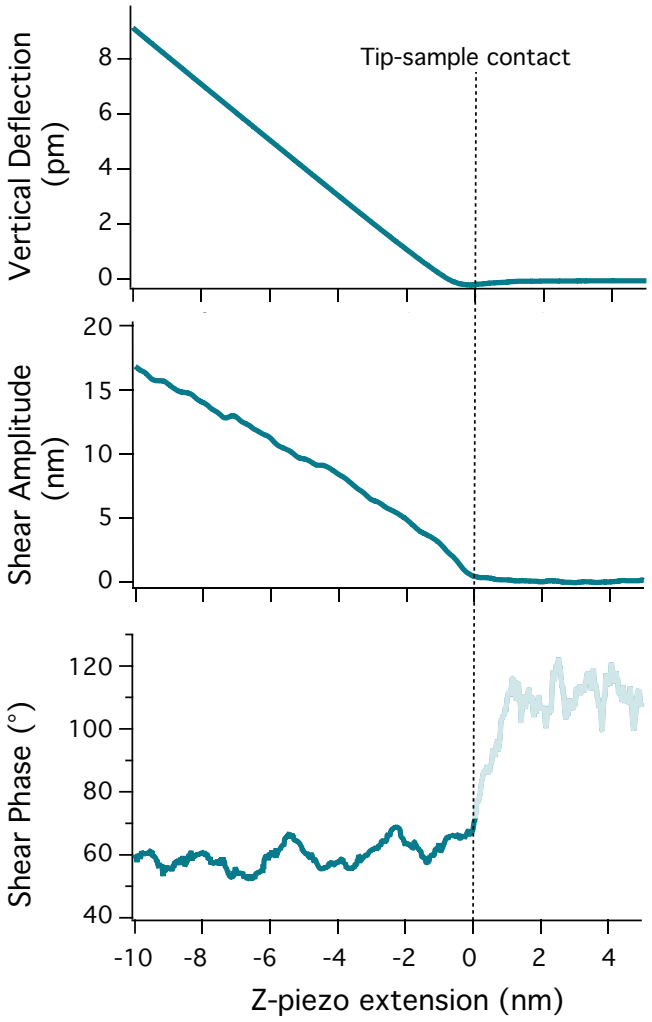

Figure S1. Example of an averaged single shear-force measurement performed in an aqueous solution of RbCl 5.0 mM, at pH 5.38 and at 25.0 °C. The vertical deflection (top subplot), shear amplitude (middle subplot) and shear phase (bottom subplot) are acquired simultaneously and shown as functions of the cantilever base vertical extension. At 0 nm (dotted vertical line), the tip begins to experience a permanent vertical deflection, defined arbitrarily as the point of contact between the tip and the sample. The semi-transparent region in the bottom subplot indicates unreliable phase data due to the associated amplitude being too small.

When the tip is nanometres away from the surface, no coupling exists between the tip and the moving solid surface; the shear amplitude is close to zero and the phase exhibits random noise. As the tip comes closer to the surface, viscoelastic coupling occurs though the liquid; the amplitude increases (here linearly) with confining force and the phase evolves rapidly, converging to a constant value (here $\varphi_t \approx 65°$), characteristic of a steady shearing regime.

6. Calibration of the shear phase offset

The shearing phase is measured with respect to a reference oscillation applied to the scanner moving the sample laterally. While in principle the scanner should move perfectly in phase with this reference signal driving its motion, in reality a delay with the reference may exist due to the practical hardware configuration. Such a delay would induce a phase offset, δ, so that even when the tip is moving completely in phase with the sample (perfectly elastic motion), the measured shear phase is δ and not zero.

In order to evaluate δ, we conducted shear experiments with the tip pinned in the sample so as to ensure a perfectly elastic coupling. Practically, this is done by applying a confining force as high as possible while shearing. The experiment was conducted in 5 mM RbCl (Fig. S2) and in water (Fig. S3) to ensure reliability of the results.

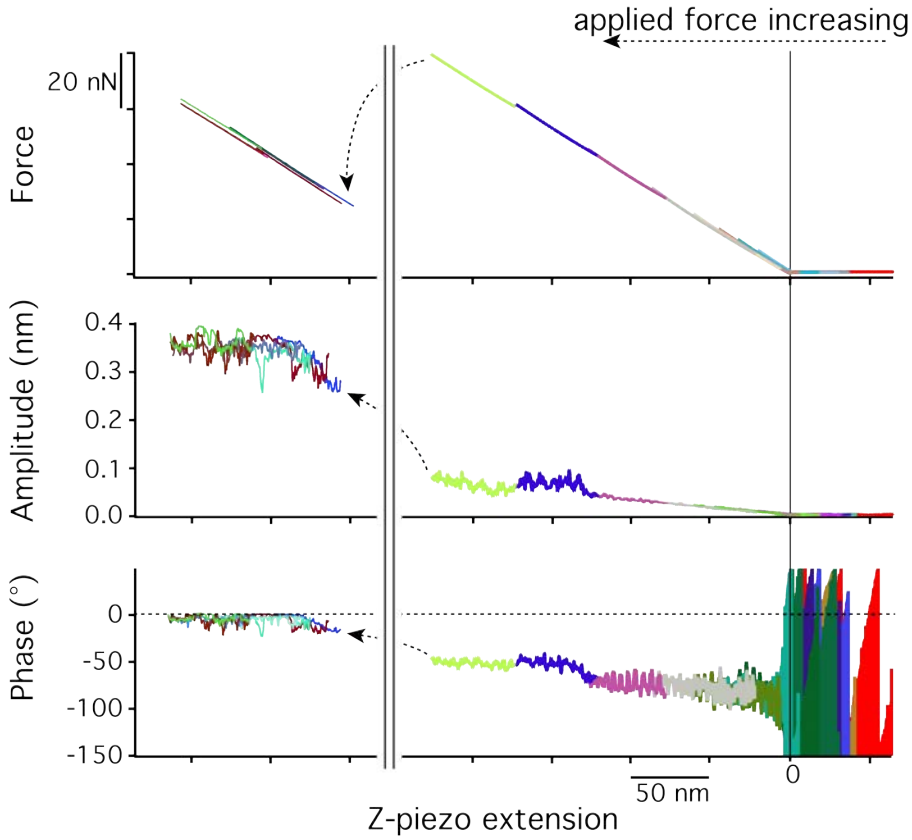

Figure S2. Shear measurement with increasing confining forces in 5 mM RbCl. The deflection (applied force), the amplitude and the phase were acquired simultaneously, using a succession of short spectroscopic curves (different colours) with the confining force progressively increasing to ensure control over the experiment. The maximum applied force (~200 nN) pins the tip into the mica (left region of the graphs). The phase in the 'pinned' region converges to zero within error (dotted line), confirming no permanent offset with the reference signal (i.e. δ=0).

The results indicate that no permanent phase offset exists between the reference and measured signal so that $\delta = 0$ and the interpretation of viscoelasticity used in this paper stands quantitatively. Given the high loads (~200 nN) applied to the tip, significant damage was done both to the tip and the sample with a local 'pit' created in the mica surface (not shown). This type of measurement was hence conducted only once in the different solutions to confirm that $\delta = 0$, regardless of the system investigated.

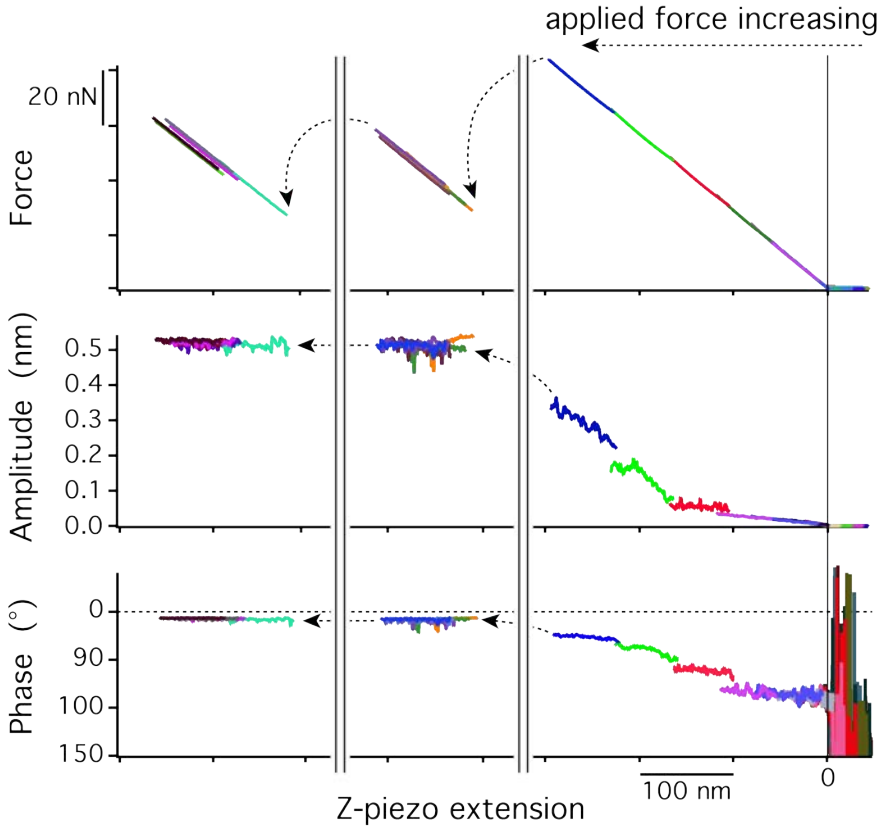

Figure S3. Shear experiment conducted with increasing confining force in ultrapure water. The deflection (applied force), the amplitude and the phase were acquired simultaneously, using a succession of short spectroscopic curves (different colours) with the confining force progressively increasing to ensure control over the experiment. The maximum force applied is in the order of ~200 nN, pinning the tip into the mica surface (left region of the graphs). The phase in the 'pinned' region converges to zero within error (dotted line), confirming no permanent offset with the reference signal (i.e. δ=0).

7. Electron microscopy analysis of the tips

In total, five cantilevers were imaged using scanning electron microscopy (SEM) after the blunting procedure, either prior or after conducting the shear-force measurements. Prior to SEM imaging, the cantilevers were gold-coated by sputtering with a 15 nm thick film to prevent charge accumulation. The images were collected using a commercial FEI Helios SEM system (Dawson Creek Drive Hillsboro, Oregon 97124 USA) operating at 5 kV electron beam in vacuum with a current set to 0.17 nA. Representative images are presented in Fig. S4. No detectable changes in the tip shape or radius of curvature before and after shearing experiments are visible within error. Since the tip is not perfectly spherical, objective determination of its radius can be problematic. Here, we use a procedure fitting the tip apex on the SEM image with circles, with the fitting weight placed either on the very apex (smaller circle) or on the overall tip (larger circles). This provides us with lower and upper estimates for the tip radius. The smallest/largest circles are shown on each figure. The procedure was repeated in magnified images of same tips to ensure its reliability and accuracy. All the radii where found between 15 nm and 19 nm (Fig. S4).

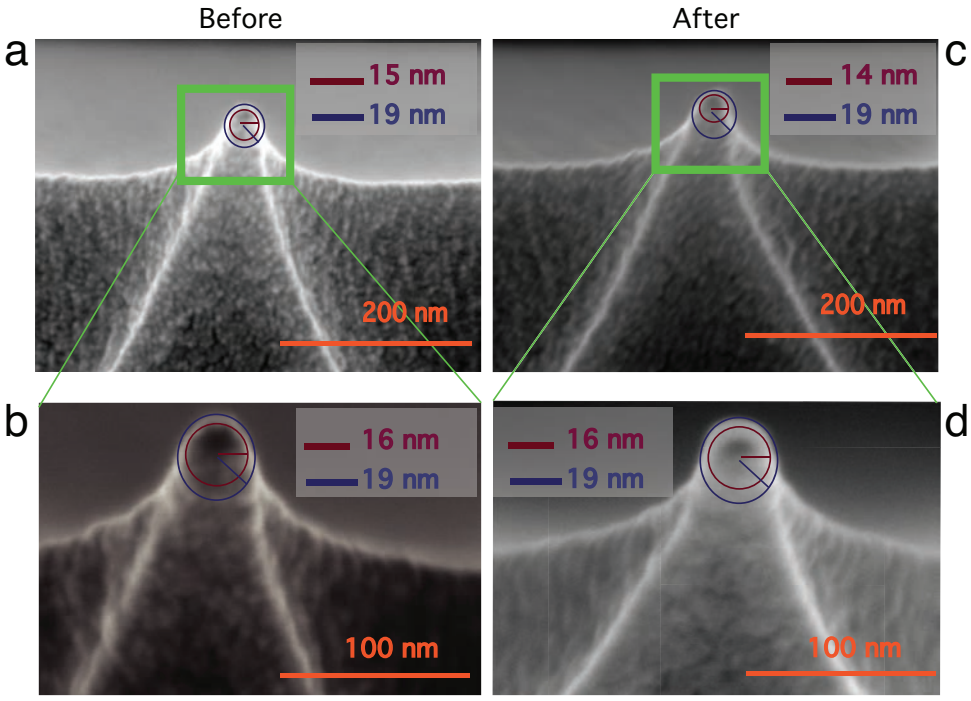

Figure S4. Representative scanning electron microscopy images showing the analysis of a selected tip. The tip is shown at different magnifications immediately after the blunting procedure but before shearing **(a-b)** and after extensive shear-force measurements **(c-d)**. The circles used to determine the lower and upper values of the tip radius are shown in each case. The radius of the blunted tip was within manufacturer's specifications.

8. Calculation of the confined solution's storage and loss moduli

The measured shear amplitude and phase can be combined to directly calculate the storage and loss moduli, (G' and G'', respectively) of the confined solution:[22]

$$G'(d) = \frac{F_{shear}\, d}{A\, X_0} \cos\phi \qquad (s4)$$

and

$$G''(d) = \frac{F_{shear}\, d}{A\, X_0} \sin\phi, \qquad (s5)$$

where F_{shear} is the shearing force, d is the tip-sample distance, A the tip-sample contact area, X_0 and ϕ the shearing amplitude and phase, respectively.

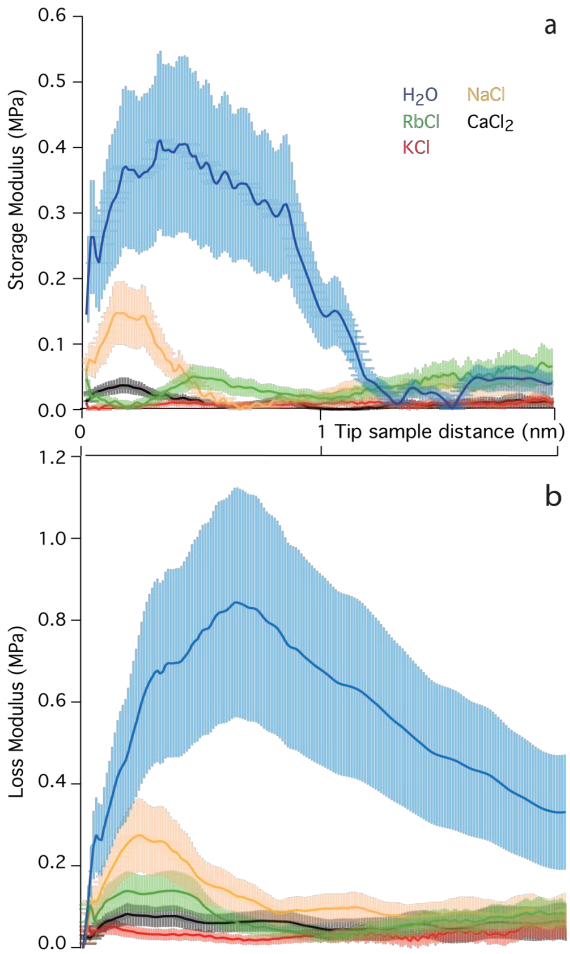

Figure S5. (a-b) Behaviour of the storage modulus, G', and loss modulus, G'', as functions of the tip-sample distance. G'' is always larger than G', as expected for a fluid material. The shearing amplitude is 0.5 nm. The area is calculated to be 10 nm^2. The slip length of hydrophilic mica was taken to be zero.[23] All the ionic aqueous solutions are at pH 5.38 and 5.0 mM. The temperature is 25.0 °C.

The storage and loss moduli for all the aqueous solutions at pH 5.38 and 5 mM are shown in Fig. S5. It is clear that G'' always dominates over G', indicating that the confined liquid preserves its fluid nature. The significant storage modulus found for ultrapure water tends to confirm the hypothesized glassy behaviour under nano-confinement. The presence of ions within the system dramatically reduces the values of G' and G''. This further illustrates the lubricating properties of the ions, even when under weak confinement.

9. Influence of pH on the shear amplitude and phase in different ionic solutions

Shear experiments were conducted at three different pH in each of the ionic solution and in ultrapure water. In all cases, only HCl was used to adjust the pH with no buffering agent to avoid interference with the measurements. The pH of the solution was checked before and after the measurements to ensure stability and no change was observed within experimental error (± 0.07). The results are presented separately for each solution at all three pH (Figs. S6-S9) to allow easier inspection.

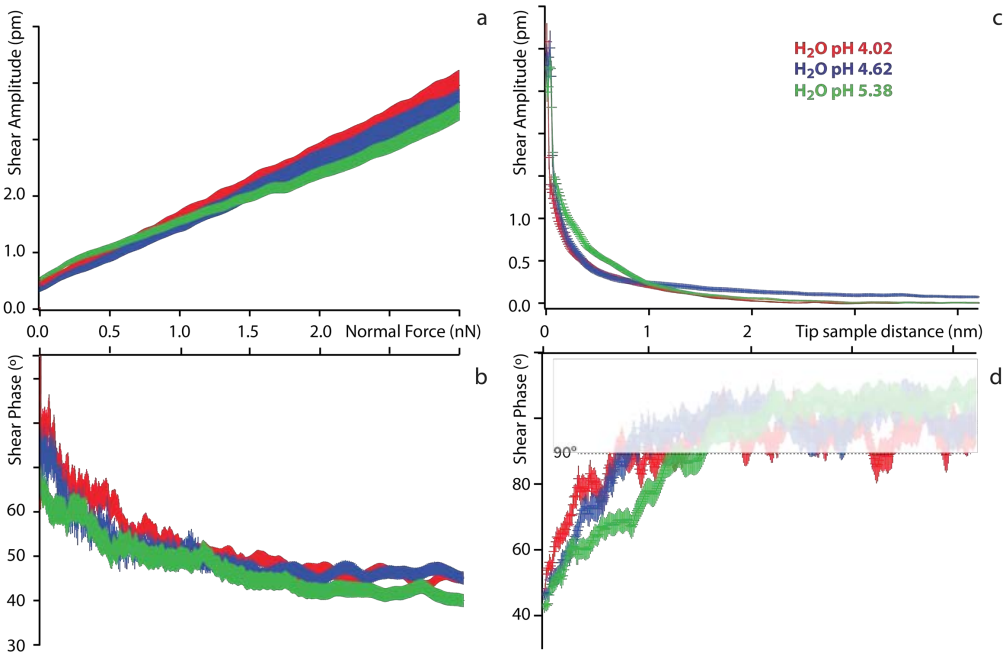

Figure S6. Averaged shear amplitude and phase as functions of the confining force (**a-b**), and of the tip sample distance (**c-d**) in ultrapure water at three different pH values. The semi-transparent region in (**d**) indicates unreliable phase due to a too small amplitude. The thickness of each curve represents the standard error.

At low confining forces (< 0.2 nN), the torsional coupling is often close to the noise level. This can result in the phase being undefined or assuming values greater than 90°. For completeness, shear phase values greater than 90° are reported but shadowed.

In ultrapure water, no significant changes in the shear amplitude with pH are visible. The absence of a clear trend differs from results in metal ions containing solutions, and is consistent with the hypothesis that the ions' size and concentration play a fundamental role in disrupting the glassy structure of the nano-confined liquid. The hydronium ion lies deep inside the ditrigonal cavities at the mica surface[24] and its hydrated radius may be too small to significantly affect the local hydrogen bond network.

In NaCl, the experiments consistently showed an unusual behaviour with the results at pH 4.62 lying outside those obtained at pH 5.38 and pH 4.02. We tentatively attribute this to the complex adsorption profile of Na^+ and the presence of multiple solvation states that may be leading to a rapid dissolution of the initial geometric hydration arrangements.[8,25]

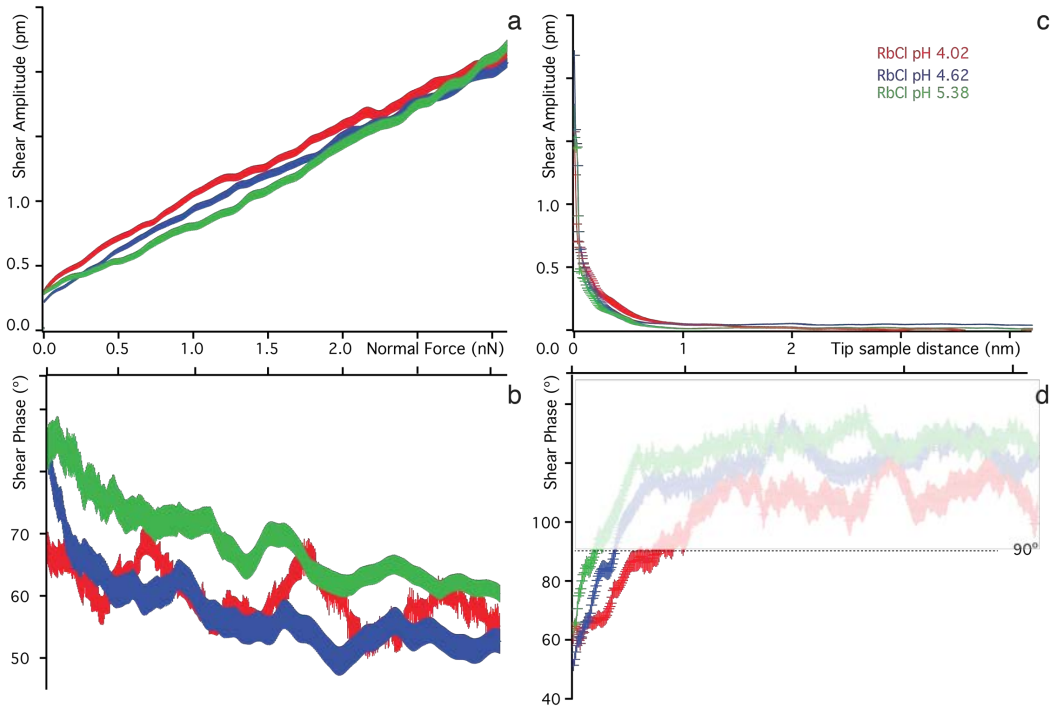

Figure S7. Averaged shear amplitude and phase as functions of the confining force (**a-b**), and of the tip sample distance (**c-d**) in RbCl 5.0 mM at three different pH values. The semi-transparent region in (**d**) indicates unreliable phase due to the shear amplitude being too small. The thickness of each curve represents the standard error.

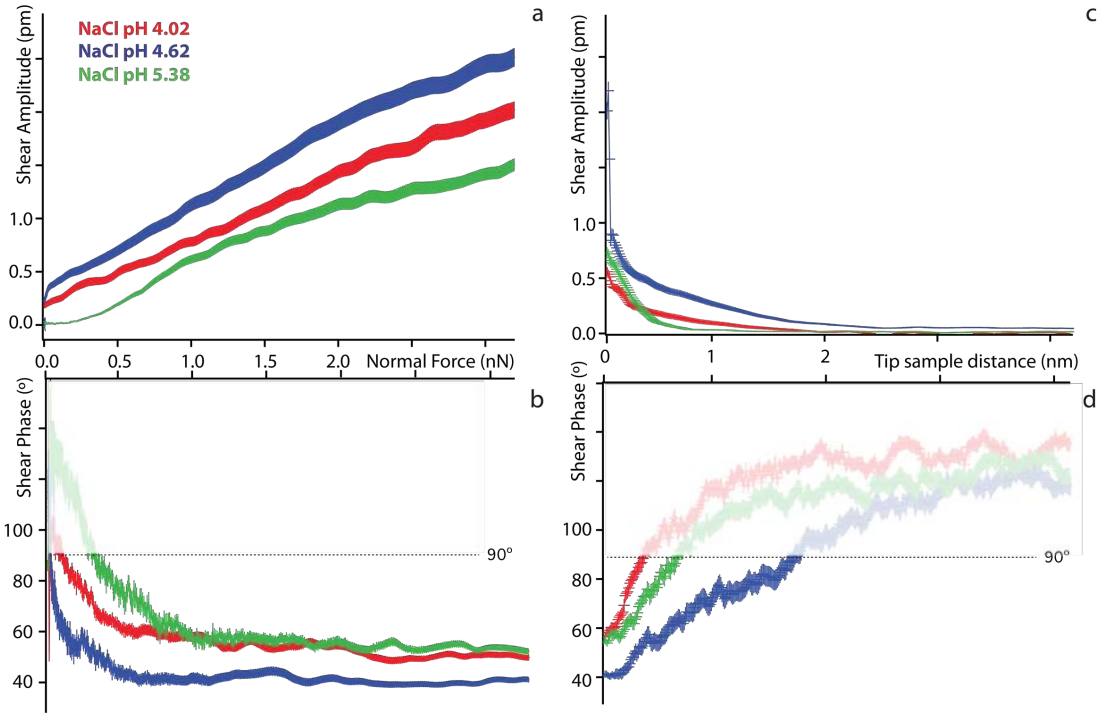

Figure S8. Averaged shear amplitude and phase as functions of the confining force (**a-b**), and of the tip sample distance (**c-d**) in NaCl 5.0 mM at three different pH values. The semi-transparent region in (**b-d**) indicates unreliable phase due to the shear amplitude being too small. The thickness of each curve represents the standard error.

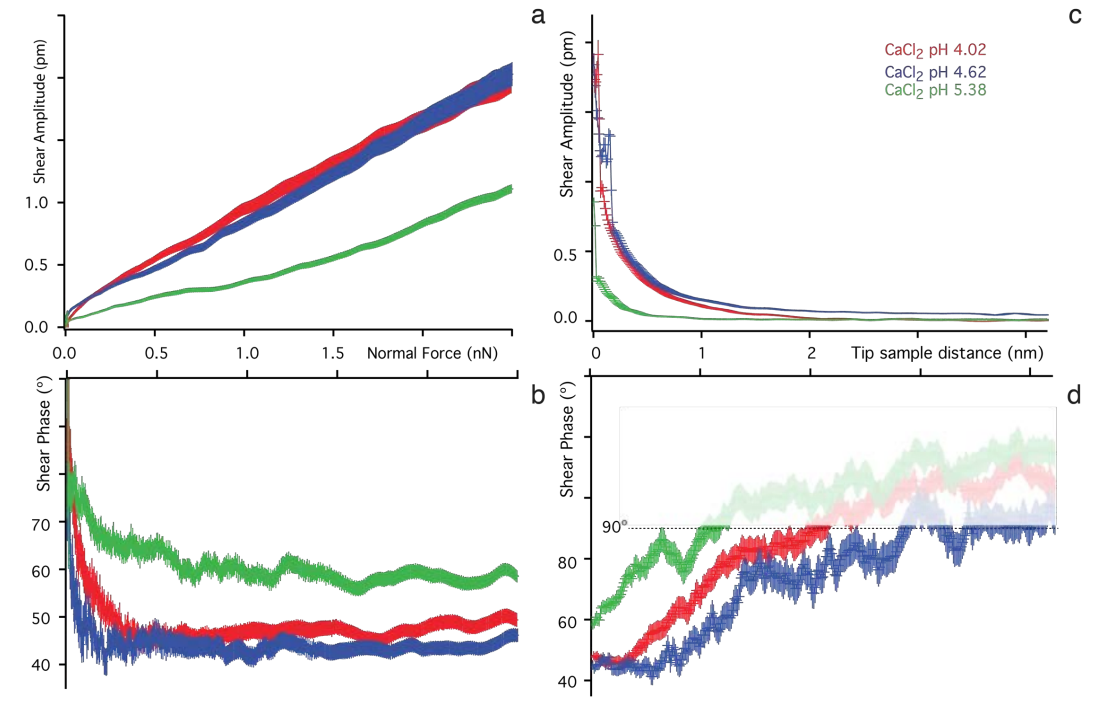

Figure S9. Averaged shear amplitude and phase as functions of the confining force (**a-b**), and of the tip sample distance (**c-d**) in $CaCl_2$ 5.0 mM at three different pH values. The semi-transparent region in (**d**) indicates unreliable phase due to the shear amplitude being too small. The thickness of each curve represents the standard error.

10. Supplementary references

1. W. Trewby, D. Livesey and K. Voïtchovsky, *Soft Matter*, 2016, **12**, 2642–2651.
2. L. Piantanida, H. L. Bolt, N. Rozatian, S. L. Cobb and K. Voïtchovsky, *Biophys. J.*, 2017, **113**, 426-439.
3. C. Park, P. A. Fenter, N. C. Sturchio and K. L. Nagy, *Langmuir*, 2008, **24**, 13993-14004.
4. H.-J. Butt and M. Jaschke, *Nanotechnology*, 1995, **6**, 1-7.
5. N. Mullin and J. K. Hobbs, *Rev. Sci. Instrum.*, 2014, **85***,* 113703.
6. C. Park, P. A. Fenter, K. L. Nagy and N. C. Sturchio, *Phys. Rev. Lett.*, 2006, **97**, 016101 (2006).
7. 7 E. J. Miller, W. Trewby, A. Farokh Payam, L. Piantanida, C. Cafolla and K. Voïtchovsky, *J. Visualized Exp.*, 2016, e54924.
8. M. Ricci, P. Spijker and K. Voïtchovsky, *Nat. Commun.*, 2014, **5**, 4400.
9. K. Voitchovsky, J. J. Kuna, S. A. Contera, E. Tosatti and F. Stellacci, *Nat. Nanotechnol.*, 2010, **5**, 401–405.
10. K. Voïtchovsky and M. Ricci, *Proc. SPIE*, 2012, **8232**, 82320O.
11. K. Voïtchovsky, *Nanoscale*, 2016, **8**, 17472-17482.
12. M. Urbakh, J. Klafter, D. Gourdon and J. Israelachvili, *Nature*, 2004, **430**, 525–528.
13. T. D. Li, H. C. Chiu, D. Ortiz-Young and E. Riedo, *Rev. Sci. Instrum.*, 2014, **85**, 123707.
14. P. Boggs and J. Rogers, *Contemp. Math.*, 1990, **112**, 183–194.
15. H. H. Ku, *J. Res. Natl. Bur. Stand.*, 1966, **70**.
16. C. P. Green, H. Lioe, J. P. Cleveland, R. Proksch, P. Mulvaney and J. E. Sader, *Rev. Sci. Instrum.*, 2004, **75**, 1988–1996.
17. C. P. Green and J. E. Sader, *J. Appl. Phys.*, 2002, **92**, 6262–6274.
18. D. R. Lide, *Handb. Chem. Phys.*, 2003.
19. J. Kestin, M. Sokolov and W. A. Wakeham, *J. Phys. Chem. Ref. Data*, 1978, **7**, 941–948.
20. M. Munz, *J. Phys. D.*, 2010, **43**, 063001.
21. D. Ebeling, D. van den Ende and F. Mugele, *Nanotechnology*, 2011, **22**, 305706.
22. T. D. Li and E. Riedo, *Phys. Rev. Lett.*, 2008, **100**, 106102.
23. D. Ortiz-Young, H.-C. Chiu, S. Kim, K. Voïtchovsky and E. Riedo, *Nat. Commun.*, 2013, **4**, 2482.
24. S. S. Lee, P. Fenter, K. L. Nagy and N. C. Sturchio, *Langmuir*, 2012, **28**, 8637-8650.
25. K. Kobayashi,Y. Liang, S. Murata, T. Matsuoka, S. Takahashi, N. Nishi, T. Sakka, *Langmuir*, 2017, **33**, 3892-3899.